Prepared for the National Institutes of Health
National Institute of Neurological Disorders and Stroke
Division of Stroke, Trauma and Neurodegenerative Disorders
Neural Prosthesis Program
Bethesda, MD 20892

Microstimulation of the Lumbosacral Spinal Cord: Mapping

NIH-NINDS-NO1-NS-8-2300

Quarterly Progress Report #11

Period Covered: 1 April, 2001 - 30 June, 2001

Principal Investigator: Warren M. Grill, Ph.D.

Co-Investigators: Kenneth J. Gustafson, Ph.D.
Musa A. Haxiu, M.D., Ph.D.
Michel A. Lemay, Ph.D.

Department of Biomedical Engineering
Case Western Reserve University
Cleveland, OH 44106-4912

ABSTRACT

The objectives of this research are to determine the anatomical locations of spinal neurons involved in control of the genitourinary and hindlimb motor systems, and to determine the physiological responses evoked in the genitourinary and hindlimb motor systems by intraspinal microstimulation. During this quarter we made progress on two different methods to map the location of spinal neurons. We continued a series of experiments using expression of the immediate early gene c-*fos* to identify neurons active during hindlimb reflexes. We continued analysis of experimental data on the hindlimb motor response evoked by microstimulation of the lumbar spinal cord, and used EMG recording to examine the role of sensory feedack in response properties. Finally, we continued our efforts to develop a method of neuronal source localization using spinal surface potential recordings, and began a comparison of our analytical and numerical models.

INTRODUCTION

Electrical stimulation of the nervous system is a means to restore function to individuals with neurological disorders. The objective of this project is to investigate the feasibility of neural prosthetics based on microstimulation of the spinal cord with penetrating electrodes. Specifically, chemical and viral retrograde tracers, immediate early gene expression, and immunocytochemistry are used to determine the locations and neurochemical identity of neurons in the spinal cord that control genitourinary and motor functions in the male cat. Microstimulation with penetrating activated iridium microelectrodes is used to determine the physiological effects in the genitourinary and motor systems of activation of different neural populations. Finally, inverse potential mapping is being explored as a method to determine, via spinal surface potential recordings, the location of active populations of neurons. The results of this project will provide data important to understanding neural control of genitourinary and motor functions, answer fundamental questions about microstimulation of the spinal cord, and lead to development of a new generation of neural prosthetics for individuals with neurological impairments.

PROGRESS IN THIS QUARTER

IDENTIFICATION OF INTERNEURONS ACTIVE DURING HINDLIMB REFLEXES

The objective of this project is to identify the location and rostrocaudal extent of spinal interneurons active during two hindlimb reflexes: flexion withdrawal and crossed extension, using expression of the immediate early gene c-Fos. The immediate early gene c-*fos* that encodes the Fos protein can be induced rapidly and transiently in post-synaptic neurons by increased electrical activity. We have completed the second series of experiments examining a flexion withdrawal response evoked via stimulation of the superficial peroneal nerve (series 1 used stimulation of the tibial nerve). The superficial peroneal nerve was stimulated to evoke a flexion withdrawal response (n=3), and a control animal (n=1) was operated, but not stimulated. Labeled spinal neurons were counted and mapped, and show areas of interneuron activation that were consistent across experimental animals.

Methods

Experimental Procedures: 4 cats were anesthetized (Ketamine/Halothane), maintained and prepared as described in QPR 10. The superficial peroneal nerve was exposed through a lateral approach and placed within a silicone rubber nerve cuff electrode.

The superficial peroneal nerve was stimulated as described in QPR 10 to induce expression of c-Fos. The hindlimb was connected to a force transducer to monitor reflex strength during the stimulation protocol. Hindlimb forces were monitored and recorded during the 2 hours of stimulation and hindlimb movement periodically monitored to verify that no reflex habituation occurred. Stimulation amplitude was increased if required.

One hour after cessation of stimulation the animals were perfused with paraformaldehyde, the lumbosacral spinal cord removed and sectioned as described in QPR 10.

The spinal cord segments were processed for the presence of Fos protein, visualized, analyzed and documented as described in QPR 10. A total of 12 sections (rostral, medial and caudal aspects of segments L5, L6, L7 and S1) were documented for each experiment.

Results and Discussion

The distribution of labeled cells was mapped by rostral-caudal segmentation and Rexed's lamina on contour-type maps for data analysis and is shown in Figure 11.1. For

each cat, maps were generated for the ipsilateral (same side as stimulated nerve) and contralateral sides of the spinal cord.

Distribution of Labeled Cells: In all experiments, the ipsilateral side of the spinal cord had more labeled cells than the contralateral side. Cell counts showed that for experiments 5, 6, 7, and 8, the ispilateral side contained 68.8%, 76.5%, 56.1%, and 69.6% of the labeled cells, respectively. The number of labeled cells in Lamina X did not effect the ispilateral/contralateral distribution, as was observed in one experiment from the first group. When the labeled cells of Lamina X were removed from the comparison, 70.2%, 76.7%, 55.6%, and 69.5% of the cells were ipsilateral for experiments 5, 6, 7, and 8, respectively. The ipsilateral dominance of interneuron activity is presumably correlated to the ipsilateral motor response of the flexion withdrawal experimental group. However, it is noted that even the control experiment showed an ipsilateral bias.

There appear to be to laminar groups of labeled cells on the ipsilateral side of all experiments and the contralateral side of experiments V and VII. Few cells were observed in laminae VIII, IX, or X, however, there were labeled cells in lamina X of experiment 5.

In each experiment, the labeled cells extended the full rostral-caudal range that was examined (Segments L5 to S1) on both the ipsilateral and contralateral sides.

Response Level: The number of labeled cells observed in the stimulated experiments (719, 425 and 194 in experiments 5, 6 and 8 respectively) was not consistently greater than the control experiment (380 in experiment 7). The number of labeled cells observed in the control experiment (380) is also greater than that observed in the control experiment with the first group (170). The number of labeled cells observed in the superficial peroneal stimulated experiments was generally less than that observed in the tibial nerve stimulated experiments that demonstrated a response (948, 196 and 1862).

The inter-animal variability in the number of observed cells is greater than expected, therefore additional sections within each spinal sub-segment will be counted. This variability was observed despite the verification of the flexion withdrawal response during stimulation.

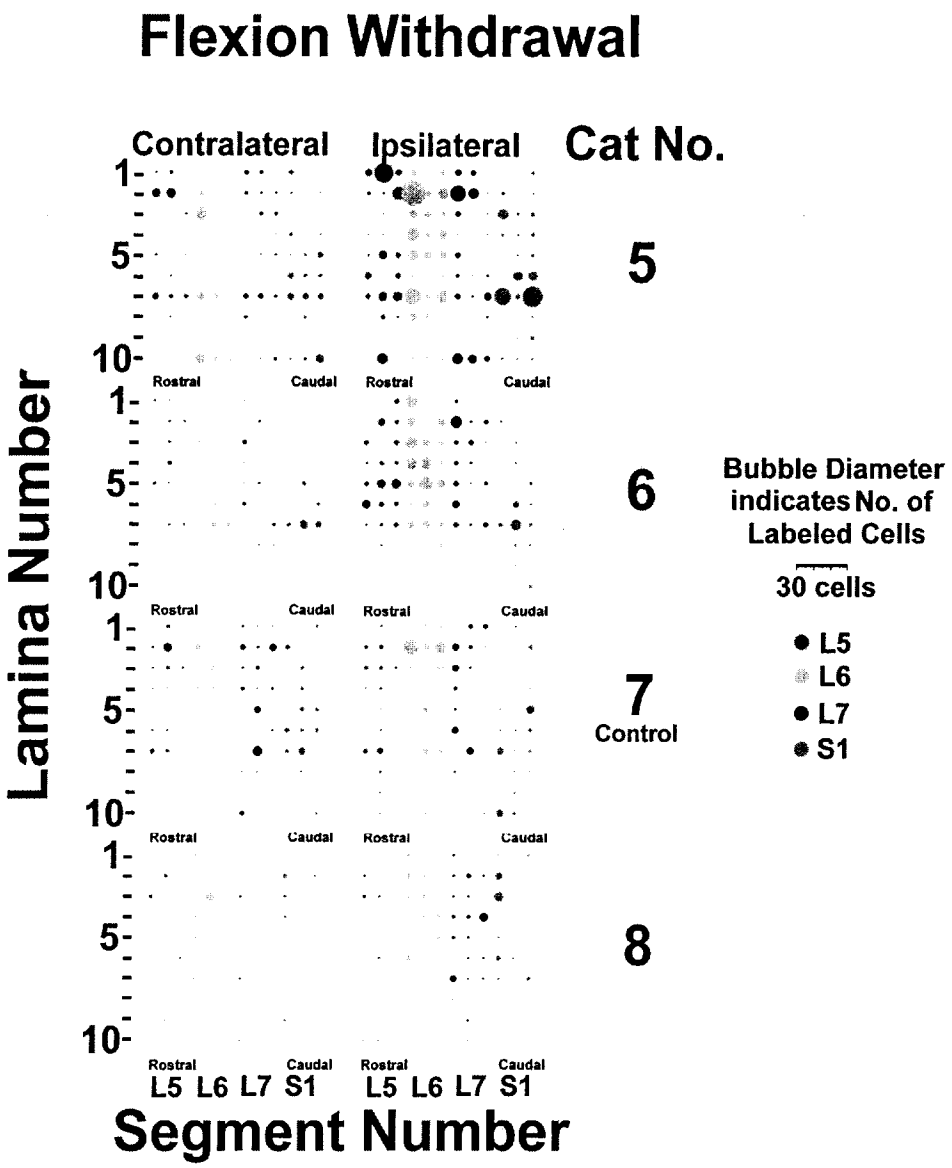

Figure 11.1 Map showing the numbers of labeled cells as well as their contralateral-ipsilateral, rostral-caudal, and laminar distributions for the four superficial peroneal stimulation experiments (5–8). The diameter of each dot codes the number of neurons expressing c-Fos immunoreactivity. Experiment 7 was an operated unstimulated control experiment.

HINDLIMB MOTOR RESPONSES EVOKED BY MICROSTIMULATION OF THE LUMBARSPINAL CORD

During this quarter we continued analysis of the intramuscular electromyographic (EMG) measurements collected during intraspinal microstimulation of the lumbar spinal cord. These measurements were obtained with the femur and hip fixed, and the paw attached to a gimball mounted on a rail manipulator that allowed us to move the end-point of the hindlimb in the sagittal plane. By measuring forces at a number of end-point positions we determined the forces produced at the paw by intraspinal microstimulation of the lumbar spinal cord. We recorded the EMG activity of four hindlimb muscles simultaneously with endpoint forces: one knee flexor, one knee extensor, one ankle dorsiflexor (TA), one ankle plantarflexor (MG). In this quarter we analyzed the influence of limb configuration on the EMG signals.

Data Analysis Methods and Results

Experimental Review

End-point force measurements were made during intraspinal microstimulation in the cat lumbar spinal cord (see previous quarter reports for description of the surgical techniques and stimulation). The pelvis and femur were held with bone pins, and the paw was attached to a gimball mounted on a multi-axis force transducer. The force transducer was mounted on an X-Y table. The table's plane of motion was oriented with the animal's sagittal plane, and forces were measured at 9-12 locations in the limb's workspace. The measured forces were represented as force fields by drawing the sagittal components of the force vectors at the measurement locations. Forces at intermediate points were obtained by dividing the workspace into triangles (with the measured locations as vertices), and interpolating the force vectors within a triangle based on the force vectors measured at the vertices.

The force patterns obtained by stimulating 67 different spinal sites in six animals were of four types. We obtained flexion withdrawal responses that pulled the limb toward the body (the typical flexion withdrawal posture), caudal extensor responses that extended the limb backward, rostral extensor responses that extended the limb forward, and one rostral flexor response that flexed the limb forward. Flexion withdrawal responses were the most common (35 of 67 fields), while rostral flexion responses were the least common (1 of 67 fields). Extensor responses fell in between these two: 21 of 67 were caudal extensor responses, and 10 of 67 were rostral extensor responses.

EMG Recording and Analysis

The EMG activity of four hindlimb muscles was recorded simultaneously with the forces. Intramuscular EMG activity was recorded with fine bifilar electrodes (Axon Engineering, Inc.) inserted into the muscles of choice. The muscles of choice were the

biceps femoris (BF), *vastus lateralis* (VL, VM), *tibialis anterior* (TA), and *medial gastrocnemius* (MG). Electrode location was verified via post-mortem dissection; the *extensor digitorum longus* (EDL) was implanted instead of the TA in two animals (SFF01 & SFF04), while the *semimembranosus* (SM) was implanted instead of the VL in one animal (SFF03). The raw EMG signal was amplified, filtered (10-1000Hz), and sampled at 2500Hz.

EMG data were rectified and averaged over 10ms bins. Normalized relative amplitudes were constructed by dividing a specific muscle EMG by the magnitude of the sum of maximum EMGs (from all four muscles) measured at that end-point position, irrespective of time. These normalized maps ranged from 0 to 1 and described the relative amplitude of each muscle's EMG with respect to the total EMG signal.

The normalized EMGs were analyzed to determine which of the following two hypotheses best described the relation between muscle activation and limb configuration. The first hypothesis states that the coordinated activation of muscles produced by intraspinal microstimulation is best described as a feedforward control system. In that hypothesis, the activation level of each muscle is invariant with position, and the relative activation levels and the intrinsic properties of the biomechanical system are responsible for producing the force patterns observed (especially the convergent ones). The second hypothesis states that muscle activation is best described as a feedback control system. In that hypothesis, the activation level of each muscle varies with position. The force patterns observed are then the results of propriospinal mechanisms combining with the intrinsic properties of the biomechanical system to modulate the response to spinal microstimulation.

Clustering methods were used to determine whether the patterns of normalized EMGs were of a single form, i.e. the relative amplitude of each muscle's EMG through time did not vary with position, or if the form of the complete EMG vector (all muscles) varied with end-point position. The complete EMG vector (a vector formed by joining the individual muscle's EMG) was clustered with respect to position (each position forming a case) using the squared Euclidean distance between cases as the measure of dissimilarity. Two methods of hierarchical clustering were used to divide the cases: the average linkage between groups, and Ward's linkage (incremental sum of squares). Normalized EMGs whose maximum amplitude was less than 0.1 were excluded from the analysis, since their contributions were considered minimal. Their absolute magnitudes were also minimal. EMGs from muscles that were spontaneously active were also excluded. These criteria excluded the EMG patterns of 6 of the 67 force measurements; the remaining 61 EMG patterns had from 1 to 4 muscles included in the analysis.

Position dependent recording properties may confound this analysis and should be considered. EMG pick-up may vary with limb configuration as the muscle fibers whose

electrical signal is being recorded move relative to the electrode. These variations in signal pick-up are indistinguishable from variations in muscle activation. Thus, even in the absence of variation in activation level, we might conclude that muscle activation varies with position. The possibility of rejecting hypothesis #1, although it may be true is present, and will be discussed further. The possibility of accepting hypothesis #1 even though it is false, is much lower. The probability that the electrode configuration dependent pick-up for all muscles is such as to make the relative activation level appear independent is lower since it requires the simultaneous occurrence of independent events while rejecting the hypothesis depends on the occurrence of a single event (one electrode changing pick-up with configuration).

Results of Cluster Analysis

The number of clusters was determined by an analysis of the trend in the dissimilarity coefficient as clusters are joined, and a visual analysis of the dendrogram structure. A sudden jump in the value of the dissimilarity coefficient indicates that the correct number of clusters has been reached and the agglomeration process is complete, while the dendrogram provides a visual confirmation. Of the 61 EMG patterns analyzed, 14 (23%) fell into one cluster using both hierarchical clustering methods, while 28 (46%) fell into one cluster with one of the methods. The average number of clusters with the average linkage method was 1.7±0.6, and 1.7±0.5 with Ward's method. The elements of the smaller cluster(s) tended to be more at the edges of the workspace rather than in the center as shown in Figure 11.2. The size of the markers for the nine end-point positions is proportional to the frequency at which a location was a member of the smallest cluster.

The results suggest that muscle activation may be modulated by the spinal circuitry based on position. The data presented would suggest that the modulation occurs mostly at the edges of the measured workspace. Another possible interpretation is that the signal-to-electrode coupling is more affected at greater muscle length changes which would explain the changes in EMG with limb configuration. A relatively high percentage of the EMG patterns measured do not show changes in relative activation between muscles associated with changes in limb configuration.

Conclusions

Cluster analysis of EMG activity provides contradictory evidence about the shaping of the muscular activation that occurs during intraspinal microstimulation. A significant number of spinal sites seem to activate muscles in an open-loop fashion, while a number of sites may modulate the muscular activation based on limb configuration. However, these cases must be interpreted cautiously.

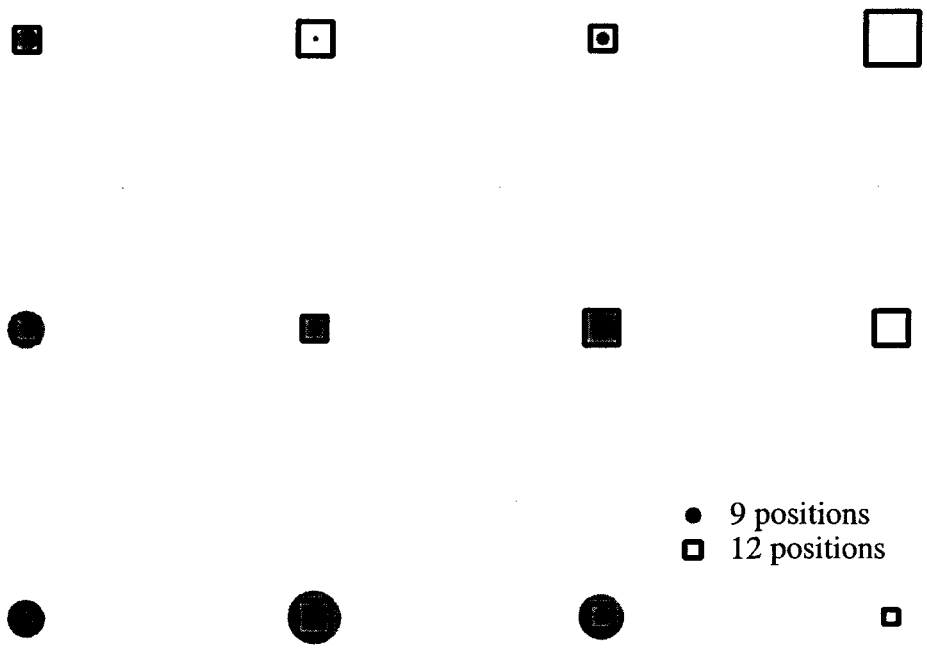

Figure 11.2 Frequency at which end-point positions fall into the smallest cluster of EMG patterns. The gray circles are for force patterns that were measured over nine end-point positions, while the black squares are for patterns that were measured over twelve end-point positions. Marker size indicates the frequency at which the EMG pattern measured at that location fell into the smallest cluster of EMG patterns. Note how the larger markers tend to be at the edges of the workspace.

DEVELOPMENT OF AN INTRAOPERATIVE SPINAL CORD MAPPING PROCEDURE

The long-term project goal is to map active motor nuclei of the spinal cord using potential recordings on the dorsal surface of the cord. We have proposed to solve this inverse problem by using a forward model in conjunction with an optimization algorithm. The forward model of the spinal cord allows us to prescribe the location of the source and solve for the resulting potentials on the model surface. The optimization algorithm compares the forward model surface potential output with the actual surface potential data and iteratively adjusts the location of the source in the forward model, attempting to minimize the difference between the actual data and the forward model output. When that minimum is found, the location of the source in the forward model will be compared to the actual source location to evaluate the degree of success. The ongoing development

of the forward model and the optimization algorithm have been described in previous progress reports.

The success of the inverse model-based approach is dependent on the quality of the forward model. In this report, we describe a preliminary comparison between the analytical model that was developed with a finite element model (FEM) that has a more realistic geometry. The purpose of this comparison is to understand the effect of the geometric simplifications of the analytical model on the spinal cord surface potential output.

Methods

Analytical Model Review: In previous progress reports, we described the development of an analytical model of the spinal cord for use in the source localization approach. The model, depicted in Figure 11.3, is composed of two concentric cylinders of infinite length located in an infinitely extending bath. The inner cylinder represents the gray matter (GM) and has isotropic conductivity, and the outer cylinder represents the white matter (WM) and has anisotropic conductivity, consistent with experimental results in the cat [Ranck and BeMent, 1965]. The electrical properties of the GM, WM(transverse), WM(longitudinal), and the bath were σ_i= 0.2 S/m, σ_o(transverse)= 0.083333 S/m, σ_o(longitudinal)= 0.5 S/m, σ_e= 1.8182 S/m respectively.

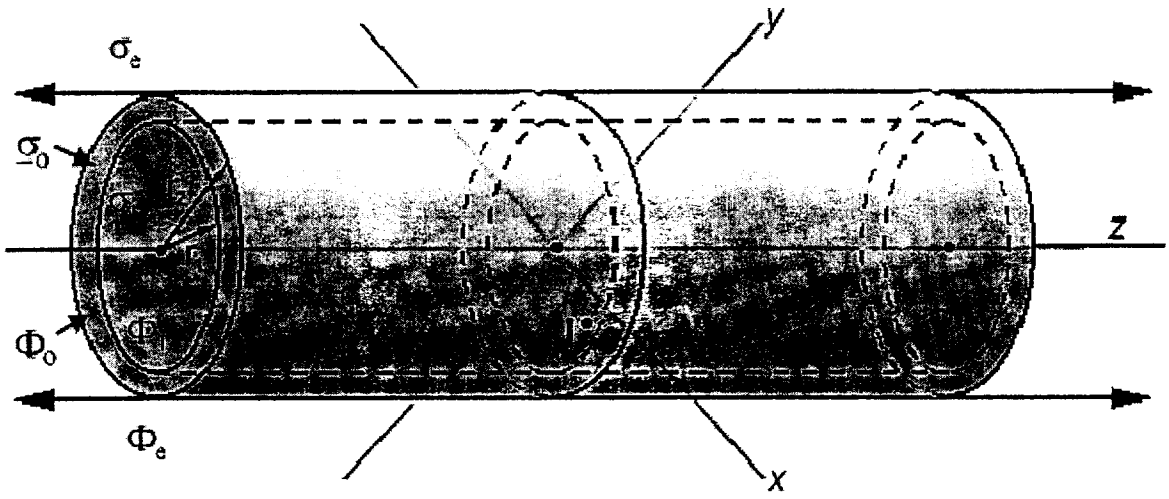

Figure 11.3: An analytical model of the spinal cord. The inner cylinder represents the gray matter and the outer cylinder represents the white matter. The cylinders are infinite in length and are surrounded by an infinite bath.

Finite Element Model: The finite element model was generated using the software package ANSYS. The 2-D geometry of the model was taken from [McIntyre & Grill, 2001]. A finite element mesh was generated in 2-D space and was then extruded 6cm to generate the 3-D model. A bath of radius 7mm surrounded the spinal cord model. The GM, WM, and bath electrical properties were assigned the same values as used in the analytical model. In both the FEM and the analytical model a monopolar current source (1μA) was used to generate surface potentials.

Comparison Strategies: To compare FEM and analytical model results, the size of the analytical model must be chosen, and the FEM and analytical models must be aligned. Two comparison strategies from the preliminary study are presented.

First, we chose an analytical model whose GM consisted of the smallest cylinder that circumscribed the GM of the finite element model (see Figure 11.4, Model Geometries). This analytical model was chosen so that any possible source location in the FEM model (sources were permitted to be located in the GM region), would have a corresponding location in the GM region of the analytical model. The models were aligned during the circumscribing of the gray matter region of the FEM by the inner cylinder of the analyitical model, and the center point was chosen to be the center of the analytical model. The determine the radius of the outer cylinder of the analytical model, we constrained the ratio of WM:GM to be the same for both models.

Second, an analytical model was generated whose GM and WM areas were equal to the respective areas of the FEM (see Figure 11.5 – Model Geometries). This strategy was chosen to give us a better surface potential match between models, acknowledging that the many possible source positions in the ventral horn of the GM of the FEM, did not have corresponding positions in the GM of the analytical model. The models were aligned by choosing the geometric center of the FEM to be the center of the analytical model. In this second scenario, a source location was chosen that fell within the GM regions of both the FEM and analytical models. This location was closer to the center of the models than the source location used in the first scenario.

To compare surface potential results, each spinal cord surface point was assigned a (θ,z) positions. The transverse section containing the source was defined to be $z=0$, and all other z-positions were defined relative to that plane. θ-coordinates were defined as radial projections from the chosen center point, with $\theta=0$ chosen to be directly dorsal from the center. Normalized surface potential maps for the analytical and finited element models of each of the above scenarios were generated by dividing surface potential amplitudes by the maximum amplitude in each case.

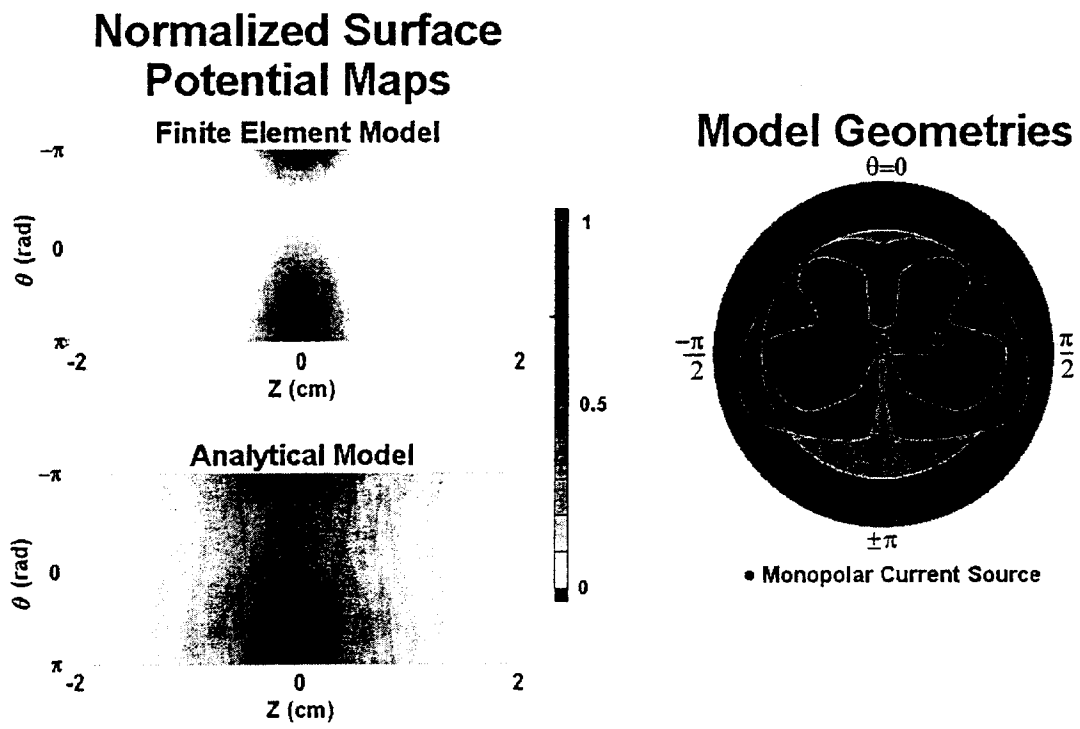

Figure 11.4: The normalized surface potential maps from the FEM and analytical models of the first comparison scenario are shown. Notice that the GM region of the analytical model circumscribes that of the FEM.

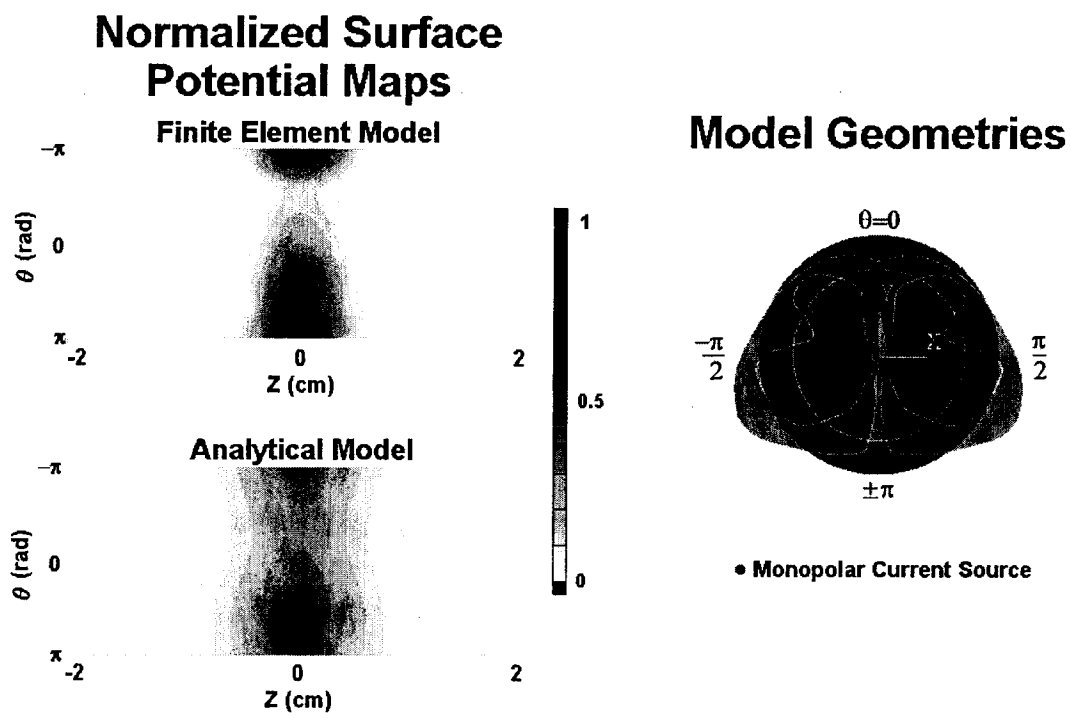

Figure 11.5 The normalized surface potential maps from the FEM and analytical models of the second comparison scenario are shown. Notice that the two model cross-sections are of equal area. Similarly, the GM regions and the WM regions of the two models are of equal area.

Results/Discussion

In both cases, the surface potential profiles of the analytical models had the same form as the surface potential profiles of the finite element models, but some clear differences were apparent. In the first scenario, the surface potential profile generated with the analytical model is smoother than the profile generated with the FEM. This effect is due to the source location being more centric in the analytical model than the source location in the FEM model. The relative source locations also effected the magnitude of the profiles, the more centric source having a smaller magnitude (peak magnitude of the analytical model was 29 μV, peak magnitude of the FEM model was 56 μV). Evidence confirming that relative source location was the cause of the smoothing effect was the absence of smoothing in the second scenario. Similarly, such a large difference in peak magnitudes was not seen in the second scenario (peak magnitude of the analytical model was 55 μV, peak magnitude of the FEM was 43 μV).

Other differences were seen in both comparison scenarios. First, the FEM surface potentials changed rapidly across the cleft between the ventral horns, and the cleft not was not present in the analytical model. However, changes in potential on the dorsal aspect of the cord where recordings are made for source localization were quite similar in both models. Second, the higher potential region in the contour maps of the finite element model profiles had an irregular shape, particularly noticeable as the potential drops from the peak magnitude in the θ=0 direction. We suspect this was an artifact from the projection method used to assign θ-positions, but it may have been due to geometrical differences between the FEM and analytical models. Third, there was a slight θ-shift in the profile peaks that can be seen when comparing the FEM profiles with the analytical model profiles. This effect was likely caused by the projection method used to assign θ-positions.

In summary, the preliminary results show that the surface potential profiles of the analytical model and a finite element model are qualitatively similar. The geometrical difference between the models that translated to the most significant difference in surface potential profiles was the cleft between the ventral horns in the FEM. Some differences, such as the θ-shift and the irregular peak shape in the surface potential profile shape appeared to be caused by the projection methods used to compare the two models, but could also have been due to geometrical differences between the FEM and analytical models.

PUBLICATIONS THIS QUARTER

Moffitt , M.A., W.M. Grill (2001) Source localization using spinal cord surface potentials and model-based optimization. Proceedings of the 6th Annual Meeting of the International FES Society, 326-328.

OBJECTIVES FOR THE NEXT QUARTER

During the next quarter we will continue experiments to identify interneurons active during hindlimb reflexes. Specifically, we will conduct crossed extension experiments using stimulation of either the tibial or superficial peroneal nerve. In addition, we will analyze additional sections from the completed experiments.

We will also continue our analysis of the EMG activity generated in hindlimb muscles by intraspinal microstimulation. Specifically, we will investigate correlation

between sites showing modulation of muscular activation and force pattern type, depth of penetration, spinal site location, and presence or absence of a point-of-zero active force.

We will continue evaluation of our methods to use electrical recordings to localize active neurons in the spinal cord. Specifically, we will complete analysis of the FEM model and quantify the effect of surface potential sampling density on the accuracy of source localization.